CLNS 01/1768

CLEO RESULTS: B DECAYS

DAVID G. CASSEL
Newman Laboratory, Cornell University, Ithaca, NY 14853, USA
E-mail: dgc@lns.cornell.edu

Measurements of many Standard Model constants are clouded by uncertainties in nonperturbative QCD parameters that relate measurable quantities to the underlying parton-level processes. Generally these QCD parameters have been obtained from model calculations with large uncertainties that are difficult to quantify. The CLEO Collaboration has taken a major step towards reducing these uncertainties in determining the CKM matrix elements $|V_{cb}|$ and $|V_{ub}|$ using new measurements of the branching fraction and photon energy spectrum of $b \to s\,\gamma$ decays. This report includes: the new CLEO measurements of $b \to s\,\gamma$ decays, $|V_{cb}|$, and $|V_{ub}|$; the first results from CLEO III data – studies of $B \to K\pi$, $\pi\pi$, and $K\bar{K}$ decays; mention of some other recent CLEO B decay results; and plans for operating CESR and CLEO in the charm threshold region.

1 Introduction

New results from CLEO include measurements of:

- the branching fraction and photon energy spectrum of $b \to s\,\gamma$ decays,
- $|V_{cb}|$ from moments of hadronic mass in $\bar{B} \to X_c \ell \bar{\nu}$ decays and photon energy in $b \to s\,\gamma$ decays,
- $|V_{ub}|$ from the spectra of lepton momentum in $\bar{B} \to X_u \ell \bar{\nu}$ decays and photon energy in $b \to s\,\gamma$ decays,
- $|V_{cb}|$ from $\bar{B} \to D^* \ell \bar{\nu}$ decay, and
- branching fractions and upper limits for the charmless hadronic decays $B \to K\pi, \pi\pi$, and $K\bar{K}$ decays from CLEO III data.

This report includes these measurements, mention of some other recent CLEO results and discussion of future plans for operating CESR and CLEO in the charm threshold region. At this conference Belle [1] and BABAR [2] also presented experimental results on some of these topics, and many of the theoretical issues were discussed by Neubert [3], Barbieri [4], Wise [5], and Isidori [6].

Common goals of all B physics programs include: identifying B decay modes and accurately measuring B branching fractions and the CKM matrix elements $|V_{cb}|$, $|V_{ub}|$, $|V_{td}|$, and $|V_{ts}|$. Figure 1 illustrates the variety of the B meson decays that can contribute to measurements of CKM matrix elements and the unitarity triangle. However, the importance of B decays arises from the possibility that the key to understanding CP violation can be found in the b quark sector. Earlier today BaBar [7] and Belle [8] reported major advances in this direction – statistically significant measurements of the CP violating parameter $\sin(2\beta)$, where the angle β is illustrated in Figure 1.

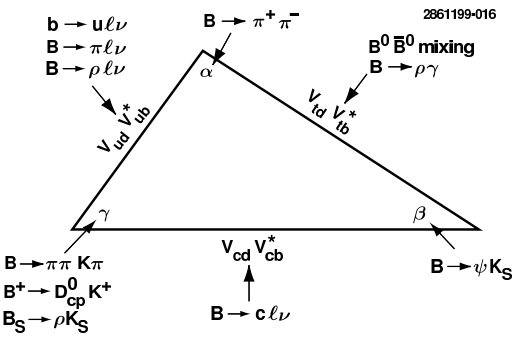

Figure 1. The unitarity triangle and some of the B meson measurements that can contribute to determining the angles and CKM matrix elements.

According to conventional wisdom the amount of CP violation in the Standard Model (*i.e.*, in the CKM matrix) is not sufficient to account for the observed matter-antimatter asymmetry in the universe. Hence, major goals of B physics pro-

To be published in the
Proceedings of the XX International Symposium on Lepton and Photon Interactions at High Energies
Rome, July 23 – 28, 2001

grams also include searches for CP violation and other New Physics beyond the Standard Model (SM). Phenomena beyond the SM may appear in B decays involving loops, such as rare charmless hadronic B decays and $b \to s\,\gamma$ decays. Accurate measurement of CKM matrix elements and searches for new physics beyond the SM are the principal priorities of the CLEO B physics program.

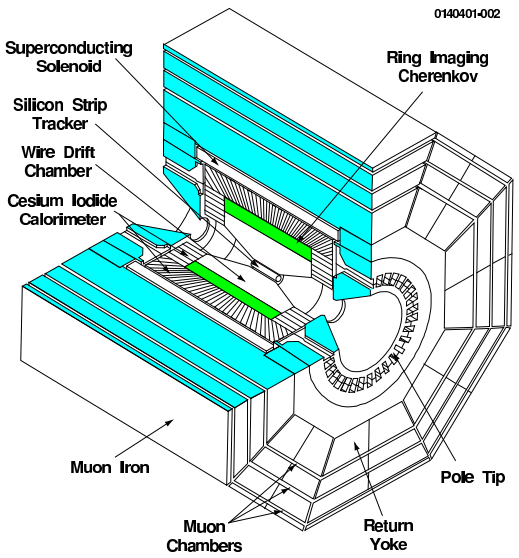

Figure 2. The CLEO III detector.

2 The CLEO Detectors and Data

We obtained the B decay results reported here using three configurations of the CLEO detector, called CLEO II, CLEO II.V, and CLEO III. The CLEO III detector is illustrated in Figure 2. The CsI calorimeter, superconducting coil, magnet iron, and muon chambers are common to all three detector configurations. In the CLEO III upgrade, the CLEO II.V silicon vertex detector, drift chamber and time of flight counters were replaced by a new silicon vertex detector, a new drift chamber, and a new Ring Imaging Cherenkov detector, respectively. Table 1 describes the performance achieved with the CLEO III detector.

Table 1. CLEO III detector performance.

Component	Performance
Tracking	93% of 4π; at $p = 1$ GeV/c $\sigma_p/p = 0.35\%$; dE/dx resolution 5.7% for minimum-ionizing π
RICH	80% of 4π; at $p = 0.9$ GeV/c 87% kaon efficiency with 0.2% pion fake rate
Calorimeter	93% of 4π; $\sigma_E/E =$ 2.2% at $E = 1$ GeV 4.0% at $E = 0.1$ GeV
Muons	85% of 4π for $p > 1$ GeV/c
Trigger	Fully pipelined; Latency ~ 2.5 μs; Based on track and shower counter topology
DAQ	Event Size: ~ 25 kByte; Throughput $\sim$ 6 MB/s

Table 2. The numbers of $B\bar{B}$ events recorded and the $\Upsilon(4S)$ and continuum integrated luminosities for the three CLEO detector configurations.

Detector	$\Upsilon(4S)$ fb^{-1}	Cont. fb^{-1}	$B\bar{B}$ (10^6)
CLEO II	3.1	1.6	3.3
CLEO II.V	6.0	2.8	6.4
Subtotal	9.1	4.4	9.7
CLEO III	6.9	2.3	7.4
Total	16.0	6.7	17.1

We accumulated a total of 17.1 M $B\bar{B}$ events at the $\Upsilon(4S)$ and we devoted about 30% of our luminosity to running in the continuum just below the $\Upsilon(4S)$. These continuum data were essential for determining backgrounds for the inclusive measurements. The breakdown of the data samples among

the different detectors, the $\Upsilon(4S)$, and the continuum are summarized in Table 2. Only CLEO II data are used in the exclusive $\bar{B}^0 \to D^{*+}\ell^-\bar{\nu}_\ell$ analysis, CLEO II and II.V data are now used in most other analyses, and CLEO III data are used for the new $B \to K\pi$, $\pi\pi$, and $K\bar{K}$ results.

3 $b \to s\gamma$ Decays

The radiative penguin diagram illustrated in Figure 3 is responsible for radiative decays of B mesons. The branching fraction, $\mathcal{B}(b \to s\gamma)$, for inclusive $B \to X_s\gamma$ decays is sensitive to charged Higgs or other new physics beyond the SM in the loop, and to anomalous $WW\gamma$ couplings. Reliable QCD calculations of $\mathcal{B}(b \to s\gamma)$ in next to leading order (NLO) are available for comparison with experimental measurements. On the other hand, exclusive $B \to K^{*(*)}\gamma$ branching fractions are sensitive to hadronization effects and therefore cannot be used in reliable searches for new physics.

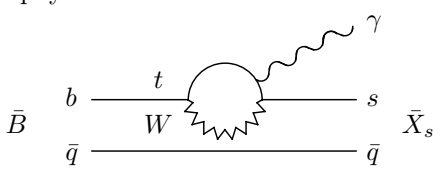

Figure 3. Radiative penguin diagram for $\bar{B} \to \bar{X}_s\gamma$ decays. The photon can couple to the W or any of the other quarks. The observed hadronic final state $\bar{X}_s$ arises from the hadronization of the s and $\bar{q}$ quarks.

Only CLEO II data were available for the original CLEO measurement [9] of $\mathcal{B}(b \to s\gamma)$. We now report an update [10] using the full CLEO II and CLEO II.V data sample; a total of almost a factor of 3 more data than were used in the earlier analysis.

The basic $b \to s\gamma$ signal is an isolated γ with energy, $2.0 < E_\gamma < 2.7$ GeV. This includes essentially all of the E_γ spectrum. Previously CLEO used only the range $2.2 < E_\gamma < 2.7$ GeV. There is much less model dependence in the new result since essentially the entire $b \to s\gamma$ spectrum is now measured.

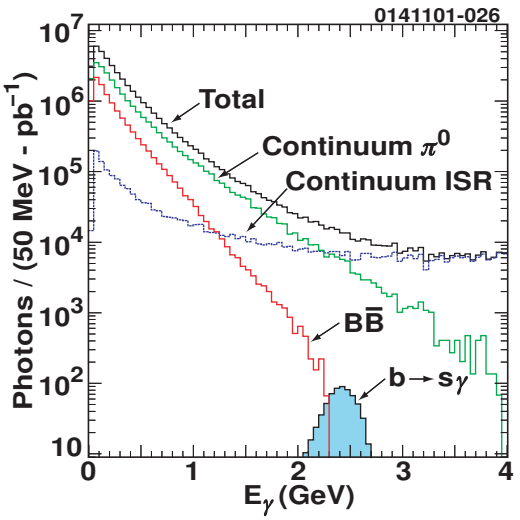

Figure 4. Monte Carlo estimate of the inclusive γ spectra from continuum and $B\bar{B}$ events.

Figure 4 shows that the $b \to s\gamma$ signal is swamped by γ's from continuum events, arising either from π^0 decays or initial state radiation (ISR). Below about 2.3 GeV, the number of γ's from other $B\bar{B}$ decays is also larger than the $b \to s\gamma$ signal.

Two basic strategies were used to reduce the huge background of γ's from continuum events: combining event shapes and the energies in cones relative to the photon direction in a neural net (NN), and pseudo-reconstruction (PR) – approximately reconstructing an X_s state from 1-4 pions and either a $K^0_S \to \pi^+\pi^-$ decay or a charged particle with ionization consistent with a $K^\pm$. For reconstructed events, the χ^2 derived from the pseudo-reconstruction was combined with other kinematic variables in a neural net. If a lepton was present in either an NN or PR event, lepton kinematic variables were also added to the appropriate neural net. Eventually four neural nets were used to handle the different cases NN and PR, with and without a lepton. Then all information from these four neural nets was combined into a single weight between 0 (continuum) and 1 ($B \to X_s\gamma$). Figure 5(a)

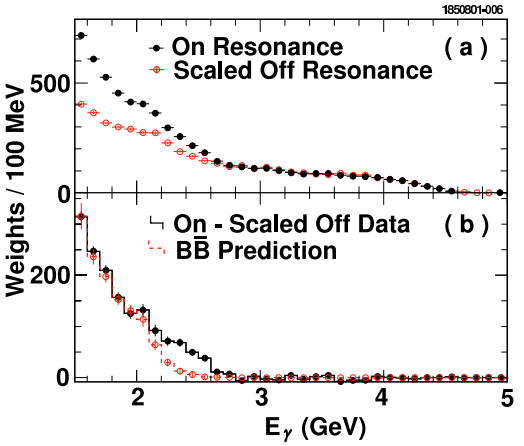

Figure 5. Distributions of weights versus E_γ for $B \to X_s\gamma$ candidate events. (a) the weight distributions for On-$\Upsilon(4S)$ events and Off-$\Upsilon(4S)$ events scaled to the same luminosity and CM energy. (b) the result of subtracting the scaled Off data from the On data and the Monte Carlo prediction of the $B\bar{B}$ contribution.

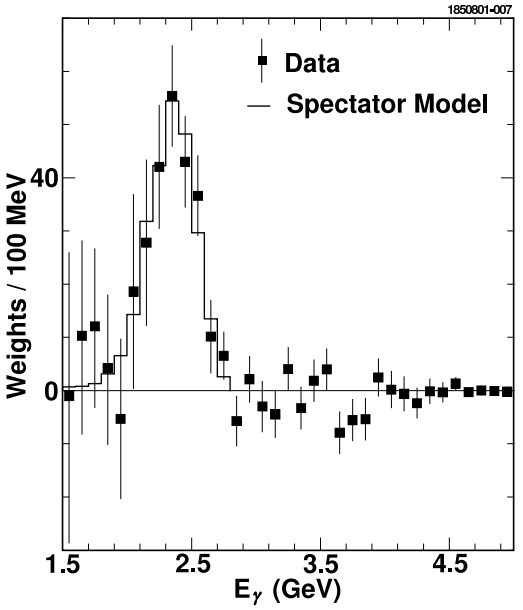

Figure 6. The observed E_γ weight distribution after subtraction of continuum and $B\bar{B}$ backgrounds. The Spectator Model spectrum is from a Monte Carlo simulation of the Ali-Greub [11] model.

shows the distributions of these weights versus E_γ for On-$\Upsilon(4S)$ and Off-$\Upsilon(4S)$ (continuum) data. Figure 5(b) shows the result of subtracting the Off data from the On data and the Monte Carlo estimate of the background from $B\bar{B}$ events. The Subtracted and $B\bar{B}$ distributions agree very well below and above the $b \to s\,\gamma$ signal region, demonstrating that the Continuum contribution has been estimated very accurately. *Clearly the large continuum data sample is essential for this analysis.*

The weight distribution after subtracting the continuum and $B\bar{B}$ background contributions is illustrated in Figure 6 along with the spectrum shape derived from a Monte Carlo simulation based on the Ali-Greub [11] spectator model. Hadronization of the $s\bar{q}$ state was modeled with K^* resonances chosen to approximate the Ali-Greub X_s mass distribution, and with JETSET tuned to the same mass distribution. (Very similar results are obtained from the Kagan-Neubert [12] theory.) After correcting the results for the $b \to d\,\gamma$ contribution and the fraction of the total $b \to s\,\gamma$ spectrum in our E_γ interval, we obtain the branching fraction

$$\mathcal{B}(b \to s\,\gamma) = (3.21 \pm 0.43 \pm 0.27^{+0.18}_{-0.10}) \times 10^{-4} \quad (1)$$

where the first error is statistical, the second is systematic, and the third is from theoretical corrections.

This CLEO measurement agrees very well with the previous CLEO result [9]. Figure 7 illustrates the excellent agreement of this result with recent ALEPH [13] and Belle [14] measurements, as well as with two NLO theoretical calculations by Chetyrkin-Misiak-Münz [15] (CMM) and Gambino-Misiak [16] (GM). The agreement of this measurement with the theoretical predictions leaves little room for New Physics in $b \to s\,\gamma$ decays.

4 Measuring $|V_{cb}|$ using Hadronic Mass Moments and $b \to s\,\gamma$

The spectator diagram for $\bar{B} \to X_c\ell\bar{\nu}$ decay is illustrated in Figure 8. The width $\Gamma^c_{SL} \equiv \Gamma(\bar{B} \to X_c\ell\bar{\nu})$ for inclusive semileptonic decay to all charm states X_c is

$$\Gamma^c_{SL} = \mathcal{B}(\bar{B} \to X_c\ell\bar{\nu})/\tau_B = \gamma_c|V_{cb}|^2. \quad (2)$$

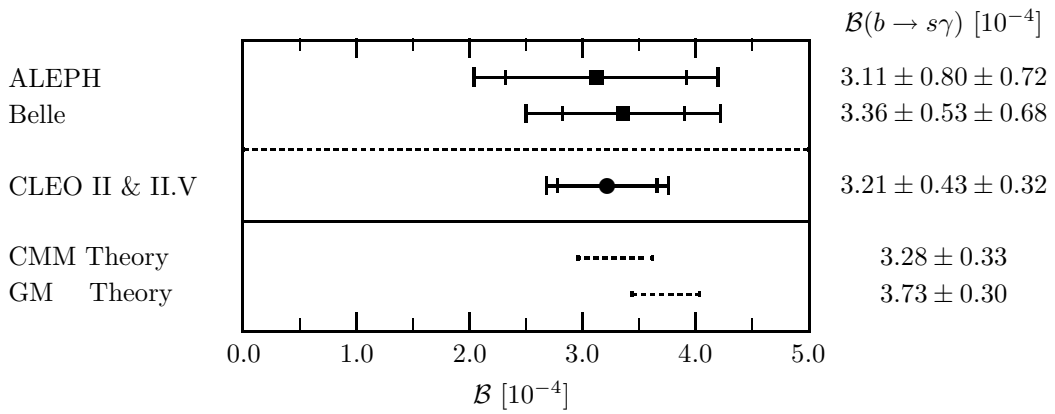

Figure 7. Comparison of the new CLEO measurement of $\mathcal{B}(b \to s\,\gamma)$ to the ALEPH [13] and Belle [14] measurements and to the CMM [15] and GM [16] Standard Model theory calculations.

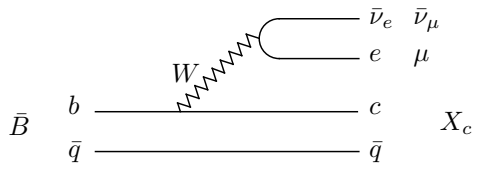

Figure 8. The spectator diagram for $\bar{B} \to X_c\ell\bar{\nu}$ decay. The same diagram with c replaced with u describes $\bar{B} \to X_u\ell\bar{\nu}$ decay.

Clearly the CKM matrix element $|V_{cb}|$ can be determined from the branching fraction for $\bar{B} \to X_c\ell\bar{\nu}$ decays, if the theoretical parameter γ_c is known. Unfortunately γ_c is a nonperturbative QCD parameter, and theoretical models have been the only means of estimating γ_c. However, measurements of hadronic mass moments in $\bar{B} \to X_c\ell\bar{\nu}$ decays combined with energy moments in $b \to s\,\gamma$ decays can essentially eliminate model dependence.

To order $1/M_B^3$ the decay width $\Gamma(\bar{B} \to X_c\ell\bar{\nu})$ can be written in the form

$$\Gamma^c_{SL} = \frac{G_F^2|V_{cb}|^2 M_B^5}{192\pi^3}\left[\mathcal{G}_0 + \frac{1}{M_B}\mathcal{G}_1(\bar{\Lambda}) + \frac{1}{M_B^2}\mathcal{G}_2(\bar{\Lambda},\lambda_1,\lambda_2) + \frac{1}{M_B^3}\mathcal{G}_3(\bar{\Lambda},\lambda_1,\lambda_2|\rho_1,\rho_2,\mathcal{T}_1,\mathcal{T}_2,\mathcal{T}_3,\mathcal{T}_4)\right] \quad (3)$$

where $\bar{\Lambda}, \lambda_1, \lambda_2, \rho_1, \rho_2, \mathcal{T}_1, \mathcal{T}_2, \mathcal{T}_3, \mathcal{T}_4$ are nonperturbative QCD parameters, the $\mathcal{G}_n$ are polynomials of order $\leq n$ in $\bar{\Lambda}, \lambda_1, \lambda_2$, and $\mathcal{G}_3$ is linear in $\rho_1, \rho_2, \mathcal{T}_1, \mathcal{T}_2, \mathcal{T}_3, \mathcal{T}_4$. Some of the coefficients of the polynomials $\mathcal{G}_n$ involve expansions in α_S.

There are similar expressions – involving the same nonperturbative QCD parameters – for the moments $\langle(M_X^2 - \bar{M}_D^2)\rangle$ of the hadronic mass (M_X) spectrum in $\bar{B} \to X_c\ell\bar{\nu}$ decay and $\langle E_\gamma\rangle$ of the energy spectrum in $b \to s\,\gamma$ decay. (Here $\bar{M}_D = 0.25M_D + 0.75M_{D^*}$, the spin-averaged D meson mass.) The coefficients $\mathcal{M}_n$ and $\mathcal{E}_n$ of the polynomials for these moments depend on the lepton momentum range measured in $\bar{B} \to X_c\ell\bar{\nu}$ decays and the energy range measured in $b \to s\,\gamma$ decays, respectively.

To obtain $|V_{cb}|$ from Eq. (3), we determined $\bar{\Lambda}$ and λ_1 from $\langle(M_X^2 - \bar{M}_D^2)\rangle$ and $\langle E_\gamma\rangle$ after: determining λ_2 from $M_{B^*} - M_B$ and estimating $\rho_1, \rho_2, \mathcal{T}_1, \mathcal{T}_2, \mathcal{T}_3, \mathcal{T}_4$ to be about $(0.5\text{ GeV})^3$ from dimensional considerations.

Moments of the E_γ spectrum in $b \to s\,\gamma$ decay were determined from the data and the spectator model illustrated in Figure 6 in the previous section. The first and second moments of E_γ obtained in this analysis are:

$$\langle E_\gamma\rangle = 2.346 \pm 0.032 \pm 0.011 \text{ GeV and} \quad (4)$$

$$\langle(E_\gamma - \langle E_\gamma\rangle)^2\rangle = 0.0226 \pm 0.0066 \pm 0.0020 \text{ GeV}^2. \quad (5)$$

The calculation of the hadronic mass M_X starts with reconstruction of the neutrino in events with a single lepton by ascribing the missing energy and momentum to the neutrino. We then use $M_X^2 \cong M_B^2 + M_{\ell\nu}^2 - 2E_B E_{\ell\nu}$ where $M_{\ell\nu}$ and $E_{\ell\nu}$ are the invariant mass and the energy of the $\ell\nu$ system, respectively. (This expression is obtained by setting $\cos\theta_{B-\ell\nu} = 0$, where $\theta_{B-\ell\nu}$ is the unmeasurable angle between the momenta of the B and the $\ell\nu$ system.) Neutrino energy and momentum resolution, and neglect of the modest term involving $\cos\theta_{B-\ell\nu}$ result in non-negligible width for the M_X distributions of $\bar{B} \to D\ell\bar{\nu}$ and $\bar{B} \to D^*\ell\bar{\nu}$ decays.

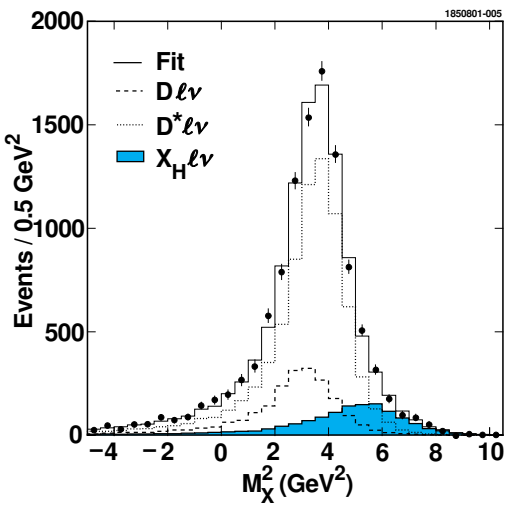

Figure 9. The measured M_X^2 distribution (points), Monte Carlo simulation (solid line), and the three components of the Monte Carlo simulation – $\bar{B} \to D\ell\nu$ (dashed), $\bar{B} \to D^*\ell\nu$ (dotted) and $\bar{B} \to X_H\ell\nu$ (shaded).

Figure 9 illustrates the experimental[17] M_X^2 distribution and Monte Carlo simulation using contributions from $\bar{B} \to D\ell\nu$, $\bar{B} \to D^*\ell\nu$, and $\bar{B} \to X_H\ell\nu$ decays, where X_H denotes high mass resonant and nonresonant charm meson states with masses above the D^*. The relative amounts of the D, D^*, and X_H contributions are determined in fits to the data. The relative rates and the generated masses are used to calculate the hadronic mass moments. The relative rates are sensitive to the model used for the $\bar{B} \to X_H\ell\nu$ spectrum, but the M_X^2 moments are quite insensitive. The dispersions in the moments for different $\bar{B} \to X_H\ell\nu$ models are included in the systematic errors for the moments. The first and second moments of M_X^2 obtained from this analysis are

$$\langle (M_X^2 - \bar{M}_D^2) \rangle = 0.251 \pm 0.023 \pm 0.062 \ \text{GeV}^2 \quad \text{and} \tag{6}$$

$$\langle (M_X^2 - \bar{M}_D^2)^2 \rangle = 0.639 \pm 0.056 \pm 0.178 \ \text{GeV}^4 \tag{7}$$

The experimental moments were measured with $E_\ell > 1.5$ GeV and $E_\gamma > 2.0$ GeV. Falk and Luke [18] calculated the coefficients of the polynomials $\mathcal{E}_n$ and $\mathcal{M}_n$ for the same ranges of E_ℓ and E_γ. We use only $\langle E_\gamma \rangle$ and $\langle (M_X^2 - \bar{M}_D^2) \rangle$ to determine $\bar{\Lambda}$ and λ_1 since theoretical expressions for the higher moments converge slowly and are much less reliable [18]. These moments define the bands in the $\bar{\Lambda}$-λ_1 plane, illustrated in Figure 10. The intersection of the bands from the two moments yields

$$\bar{\Lambda} = 0.35 \pm 0.07 \pm 0.10 \ \text{GeV} \tag{8}$$

$$\lambda_1 = -0.236 \pm 0.071 \pm 0.078 \ \text{GeV}^2 \tag{9}$$

where the errors are experimental and theoretical in that order.

The other experimental measurements we used to determine $|V_{cb}|$ are:

$$\mathcal{B}(\bar{B} \to X_c\ell\bar{\nu}) = (10.39 \pm 0.46)\% \tag{10}$$

from CLEO [19]; the ratio

$$(f_{+-}\tau_{B^-})/(f_{00}\tau_{B^0}) = 1.11 \pm 0.08 \tag{11}$$

from CLEO [20], where

$$f_{+-} \equiv \mathcal{B}(\Upsilon(4S) \to B^+B^-) \quad \text{and} \tag{12}$$

$$f_{00} \equiv \mathcal{B}(\Upsilon(4S) \to B^0\bar{B}^0); \tag{13}$$

and the PDG [21] average values of τ_{B^-} and τ_{B^0}. From this analysis we obtain

$$|V_{cb}| = (40.4 \pm 0.9 \pm 0.5 \pm 0.8) \times 10^{-3} \tag{14}$$

where the errors are due to uncertainties in moments, Γ_{SL}^c, and theory (the α_s scale and $\mathcal{O}(1/M_B^3)$ terms) in that order. This result agrees well with earlier measurements based on models, indicating that the models are reasonably adequate.

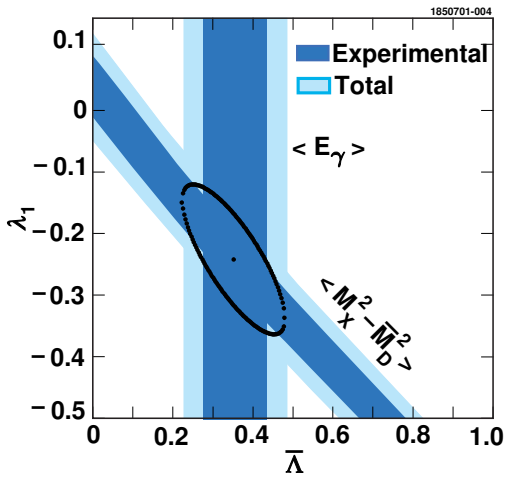

Figure 10. Bands in $\bar{\Lambda}$ and λ_1 defined by the measured $\langle E_\gamma \rangle$ and $\langle (M_X^2 - \bar{M}_D^2) \rangle$ moments. The dark gray bands indicate the experimental errors and the light gray extensions illustrate the contributions of the theoretical uncertainties.

In the question period following this report, M. Wise pointed out that moments of the lepton momentum spectrum depend on $\bar{\Lambda}$ and λ_1 and asked if we were also using these moments. Measurement of these moments is quite sensitive to systematic errors and we are working to control these errors.

5 $|V_{ub}|$ from Inclusive Leptons and the $b \to s\gamma$ Spectrum

Simply by replacing c with u, the spectator diagram (Figure 8) and the expression for the semileptonic width (Eq. (2)) that describe $\bar{B} \to X_c \ell \bar{\nu}$ decays also describe $\bar{B} \to X_u \ell \bar{\nu}$ decays. The CKM matrix element $|V_{ub}|$ can then be determined from $\mathcal{B}(\bar{B} \to X_u \ell \bar{\nu})$ and γ_u. However, measuring $|V_{ub}|$ is much more difficult because the rate of $\bar{B} \to X_u \ell \bar{\nu}$ decays is only about 1% of the $\bar{B} \to X_c \ell \bar{\nu}$ rate. Two methods have been used to measure $|V_{ub}|$: measuring the inclusive lepton momentum (p_ℓ) spectrum above or near the $\bar{B} \to X_c \ell \bar{\nu}$ endpoint or studying exclusive $\bar{B} \to \pi(\rho) \ell \bar{\nu}$ decays. So far it has not been possible to separate exclusive decays with low p_ℓ from background, so either way theory is required for the fraction $f_u(p)$ of the p_ℓ spectrum that lies in an interval (p) above some cut. Theoretical models for $f_u(p)$ have large uncertainties that are difficult to quantify, leading to severe model dependence in determining $|V_{ub}|$. However, it is possible to eliminate most of this uncertainty for inclusive $\bar{B} \to X_u \ell \bar{\nu}$ decays using $b \to s\gamma$ decays. The shape function that relates parton-level $b \to s\gamma$ decays to observed $B \to X_s \gamma$ decays also relates parton-level $b \to u \ell \bar{\nu}$ decays to $\bar{B} \to X_u \ell \bar{\nu}$ decays. The strategy for determining $|V_{ub}|$ is then to fit the E_γ spectrum (Figure 6) from the $B \to X_s \gamma$ analysis in Section 3 to a shape function [12] and then to use the shape parameters to determine $f_u(p)$ [22]. Then the $\bar{B} \to X_u \ell \bar{\nu}$ branching fraction $\mathcal{B}_{ub} \equiv \mathcal{B}(\bar{B} \to X_u \ell \bar{\nu})$ can be determined from the measured branching fraction $\Delta\mathcal{B}_{ub}(p)$ for $\bar{B} \to X_u \ell \bar{\nu}$ in the momentum interval (p), using $\mathcal{B}_{ub} = \Delta\mathcal{B}_{ub}(p)/f_u(p)$.

Figure 11 illustrates the lepton momentum spectra in the region above 2.0 GeV/c from the full CLEO II and II.V data samples. Above about 2.3 GeV/c the background is dominated by leptons and fake leptons from Off-$\Upsilon(4S)$ (continuum) events. At lower momenta leptons from $\bar{B} \to X_c \ell \bar{\nu}$ and fake leptons from hadronic $B\bar{B}$ decays dominate the background. We use the momentum interval 2.2 - 2.6 GeV/c and determine the *preliminary* partial branching fraction $\Delta\mathcal{B}_{ub}(p) = (2.35 \pm 0.15 \pm 0.45) \times 10^{-4}$, where the errors are statistical and systematic in that order. From fits to the $B \to X_s \gamma$ spectrum we obtain $f_u(p) = 0.138 \pm 0.034$, where the error includes combined experimental and theoretical uncertainties. The value of $\mathcal{B}_{ub}$ derived from these numbers is also divided by a factor of (0.95 ± 0.02) to correct for QED radiative corrections. To obtain $|V_{ub}|$ from $\mathcal{B}_{ub}$ we use

$$|V_{ub}| = \left[(3.06 \pm 0.08 \pm 0.08) \times 10^{-3}\right] \times \left[\frac{\mathcal{B}_{ub}}{0.001} \frac{1.6 \text{ ps}}{\tau_B}\right]^{\frac{1}{2}} \quad (15)$$

from Hoang, Ligeti, and Manohar [23]. (Uralt-

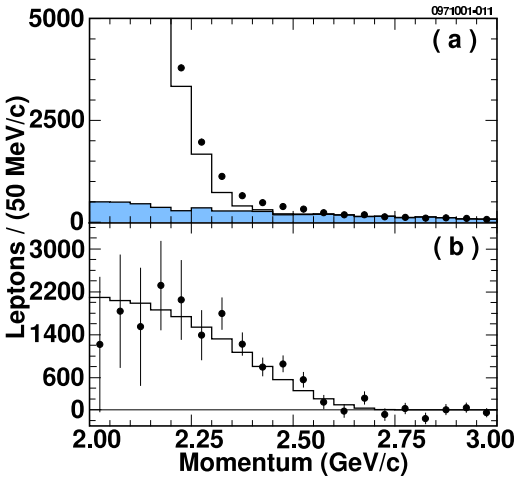

Figure 11. (a) The lepton momentum spectra for On-$\Upsilon(4S)$ data (filled circles), scaled Off-$\Upsilon(4S)$ data (shaded histogram), and sum of scaled-Off and backgrounds from B decays (solid histogram). (b) The lepton spectrum from On-$\Upsilon(4S)$ data after subtracting Off-$\Upsilon(4S)$ and $B\bar{B}$ backgrounds and correcting for efficiency (filled points) and the $\bar{B} \to X_u \ell \bar{\nu}$ spectrum derived from the $B \to X_s \gamma$ spectrum (histogram).

sev [24] obtained a nearly identical result.) The *preliminary* result is

$$V_{ub} = (4.09 \pm 0.14 \pm 0.66) \times 10^{-3} \qquad (16)$$

where the first error is statistical and the second is systematic. This result is in good agreement with previous CLEO measurements [25] based on theoretical models. Currently we are working to extend the momentum range to include as much of the $\bar{B} \to X_u \ell \bar{\nu}$ spectrum as possible, in order to minimize the residual theoretical uncertainties.

6 $|V_{cb}|$ from $\bar{B} \to D^* \ell \bar{\nu}$ Decay

Exclusive $\bar{B} \to D^* \ell \bar{\nu}$ decays provide another method for measuring $|V_{cb}|$ with experimental and theoretical uncertainties that are substantially different from those in inclusive measurements. The key to these measurements is utilization of the Isgur-Wise symmetry and Heavy Quark Effective Theory (HQET) [26]. From HQET, the differential decay width for $\bar{B} \to D^* \ell \bar{\nu}$ decay is

$$\frac{d\Gamma(w)}{dw} = \frac{G_F^2}{48\pi^3} \mathcal{G}(w) \, |V_{cb}|^2 \, \mathcal{F}_{D^*}^2(w) \qquad (17)$$

where $w \equiv v_B \cdot v_{D^*}$ (v_B and v_{D^*} are the four-velocities of the B and D^*), $\mathcal{G}(w)$ is a known function of w, and $\mathcal{F}_{D^*}(w)$ is a nonperturbative QCD form factor that parameterizes the w dependence of the hadronic current. The variable w is related to more familiar variables in $\bar{B} \to D^* \ell \bar{\nu}$ decay via

$$w = \frac{E_{D^*}}{M_{D^*}} = \frac{M_B^2 + M_{D^*}^2 - q^2}{2 M_B M_{D^*}} \qquad (18)$$

where E_{D^*} is the energy of the D^* in the B rest frame and q^2 is the momentum transfer, *i.e.*, the square of the mass of the $\ell \bar{\nu}$ system. The range of w is $(1.00 < w < 1.504)$ for $\bar{B} \to D^* \ell \bar{\nu}$ decay.

Without HQET, three unknown form factors appear in the differential decay width for $\bar{B} \to D^* \ell \bar{\nu}$. These three form factors are related by HQET, resulting in the the simple form given in Eq. (17) with only one unknown function $\mathcal{F}_{D^*}(w)$. Furthermore, for large heavy quark masses m_Q, $\mathcal{F}_{D^*}(w)$ is constrained by HQET at $w = 1$ (or $q^2_{\rm max}$) to

$$\mathcal{F}_{D^*}(1) \approx \eta_A [1 + \delta(1/m_Q^2)] \qquad (19)$$

where η_A is a perturbative QCD correction, and $\delta(1/m_Q^2)$ is a nonperturbative QCD correction of $\mathcal{O}(1/m_Q^2)$.

Hence, the ideal strategy for determining $|V_{cb}|$ using HQET would be to measure $d\Gamma(w)/dw$ at $w = 1$. However, $\mathcal{G}(1) = 0$ due to phase space, so the practical strategy is to measure $d\Gamma(w)/dw$, determine $|V_{cb}| \mathcal{F}_{D^*}(w)$ from a fit over the full w range, and extrapolate it to $w = 1$ to obtain $|V_{cb}| \mathcal{F}_{D^*}(1)$. Following Caprini-Lellouch-Neubert [27] (CLN), the dependence of $\mathcal{F}_{D^*}(w)$ on w can be reduced to dependence on two ratios of form factors $R_1(1)$ and $R_2(1)$, previously measured by CLEO [28], and a slope parameter ρ^2 to be determined in the fit.

The branching fraction for $\bar{B} \to D^* \ell \bar{\nu}$ decay and the product $|V_{cb}| \mathcal{F}_{D^*}(w)$ has been measured before [21]. We now measure these quantities with a larger data sample (3.0 fb^{-1}

of CLEO II data) and substantially reduced systematic errors. In addition, we now report results for both $\bar{B}^0 \to D^{*+}\ell^-\bar{\nu}$ and $B^- \to D^{*0}\ell^-\bar{\nu}$ decays. Previously [29], we reported results for $\bar{B}^0 \to D^{*+}\ell^-\bar{\nu}$ based on this full data sample.

We reconstruct $\bar{B} \to D^*\ell\bar{\nu}$ decays by finding D^* candidates using $D^* \to D^0\pi$ and $D^0 \to K^-\pi^+$ decays, and finding an e or a μ in the event with the same sign as the K^- and $p_e > 0.8$ GeV/c or $p_\mu > 1.4$ GeV/c. We separate the $\bar{B} \to D^*\ell\bar{\nu}$ signal from background using the angle $\theta_{B-D^*\ell}$ between the momenta of the B and the $D^*\ell$ combination. The cosine of $\theta_{B-D^*\ell}$ is

$$\cos\theta_{B-D^*\ell} = \frac{2E_B E_{D^*\ell} - M_B^2 - M_{D^*\ell}^2}{2\,P_B\;P_{D^*\ell}} \quad (20)$$

where E_B, P_B, M_B, $E_{D^*\ell}$, $P_{D^*\ell}$, and $M_{D^*\ell}$ are the energy, momentum, and mass of the B and the $D^*\ell$ system, respectively. Figure 12 shows the $\cos\theta_{B-D^*\ell}$ distributions for the w range, $1.10 < w < 1.15$. We fit the data with distributions for $D^*\ell\nu$ signals and 5 different types of backgrounds. The background shapes are determined from a combination of Monte Carlo calculations and background data samples. The combinations of signals and backgrounds fit the data very well in all w intervals.

The values of $|V_{cb}|\mathcal{F}_{D^*}(w)$ obtained from the fits to the $\cos\theta_{B-D^*\ell}$ distributions are illustrated in Figure 13 along with the fit to the $|V_{cb}|\mathcal{F}_{D^*}(w)$ data. The ingredients used in the fit are the shape of $\mathcal{F}_{D^*}(w)$ from Caprini-Lellouch-Neubert [27], $\mathcal{F}_{D^*}(w) = \mathcal{F}_{D^{*+}}(w) = \mathcal{F}_{D^{*0}}(w)$, $\Gamma(D^*\ell\bar{\nu}) = \Gamma(D^{*+}\ell\bar{\nu}) = \Gamma(D^{*0}\ell\bar{\nu})$, and the CLEO measurement [20] of the ratio $(f_{+-}\tau_{B^-})/(f_{00}\tau_{B^0})$.

From the fit to the $|V_{cb}|\mathcal{F}_{D^*}(w)$ distribution, we obtain the *preliminary* results:

$$|V_{cb}|\mathcal{F}_{D^*}(1) = (42.2 \pm 1.3 \pm 1.8) \times 10^{-3}, \quad (21)$$

$$\rho^2 = 1.61 \pm 0.09 \pm 0.21, \text{ and} \quad (22)$$

$$\Gamma(D^*\ell\bar{\nu}) = (0.037.6 \pm 0.001.2 \pm 0.002.4)\ \text{ps}^{-1}, \quad (23)$$

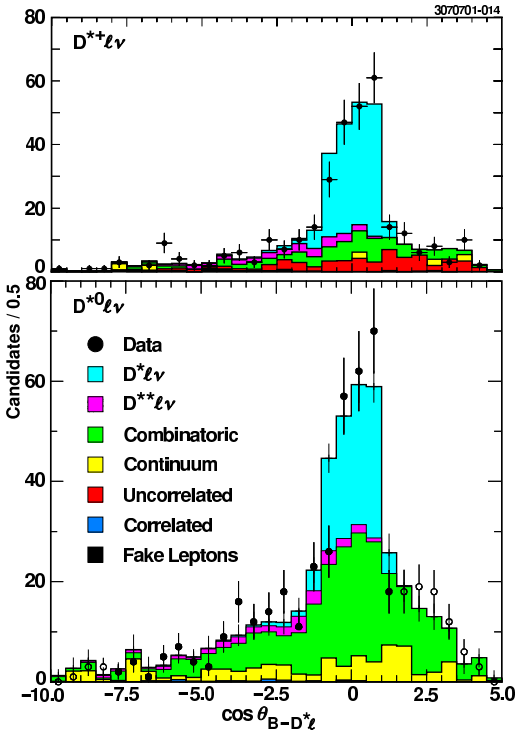

Figure 12. Distributions of $\cos\theta_{B-D^*\ell}$ for $\bar{B}^0 \to D^{*+}\ell^-\bar{\nu}$ (top) and $B^- \to D^{*0}\ell^-\bar{\nu}$ (bottom) for the w range, $1.10 < w < 1.15$. The filled circles are the data and the shaded histograms are the contributions of the $D^*\ell\nu$ signals and the backgrounds.

where ρ^2 is the slope parameter for the CLN form factor, $\mathcal{F}_{D^*}(w)$. Using the PDG [21] average lifetimes we also obtain *preliminary* branching fractions from the measured decay width, $\Gamma(D^*\ell\bar{\nu})$:

$$\mathcal{B}(D^{*0}\ell\bar{\nu}) = (6.21 \pm 0.20 \pm 0.40)\% \quad (24)$$

$$\mathcal{B}(D^{*+}\ell\bar{\nu}) = (5.82 \pm 0.19 \pm 0.37)\% \quad (25)$$

These branching fractions and the value of $|V_{cb}|\mathcal{F}_{D^*}(1)$ that we obtain are somewhat higher than and are marginally consistent with previous measurements from LEP [30].

The parameters $|V_{cb}|\mathcal{F}_{D^*}(1)$ and ρ^2 are generally highly correlated in the fits, so it is necessary to take these correlations into account in comparing results from different experiments. This is illustrated in Figure 14.

The correlation between $|V_{cb}|\mathcal{F}_{D^*}(1)$ and ρ^2 in CLEO data is less than the correlation

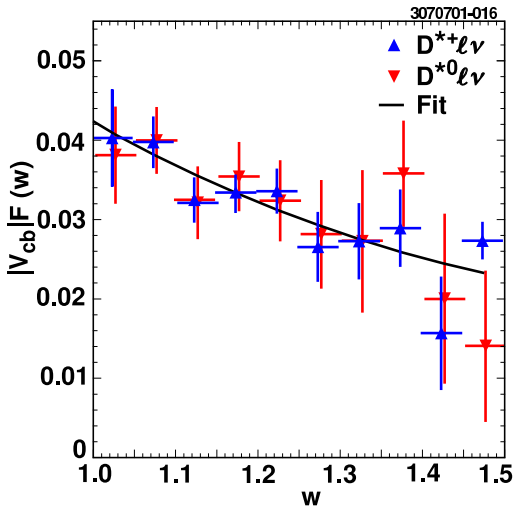

Figure 13. Values of $|V_{cb}|\mathcal{F}_{D^*}(w)$ obtained from the fits to the $\cos\theta_{B-D^*\ell}$ distributions for $\bar{B}^0 \to D^{*+}\ell^-\bar{\nu}$ (upward triangles) and $B^- \to D^{*0}\ell^-\bar{\nu}$ (downward triangles). The fit is described in the text.

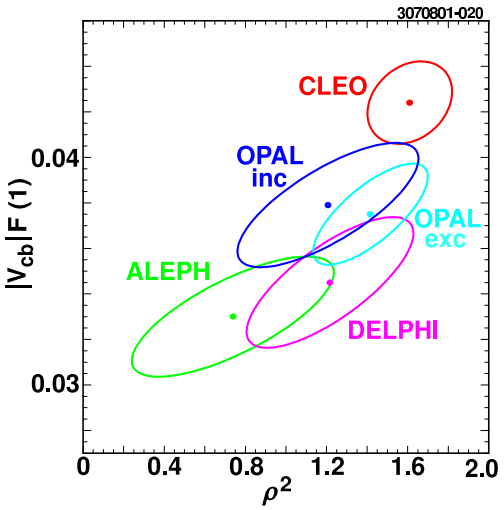

Figure 14. The correlations between $|V_{cb}|\mathcal{F}_{D^*}(1)$ and ρ^2 in CLEO and LEP [30] measurements. OPAL used a partial reconstruction of $\bar{B}^0 \to D^{*+}\ell^-\bar{\nu}$ decays for the measurement labeled OPAL inc.

in LEP data. This is due to an interaction in the systematic error between the lepton momentum cuts that we use and the measured form factor ratios $R_1(1)$ and $R_2(1)$ in the CLN form of $\mathcal{F}_{D^*}(w)$.

One possible source of the apparent discrepancy between CLEO and LEP measurements is the fact that $D^*X\ell\bar{\nu}$ components are estimated differently by the two different groups; CLEO included this component in the $\cos\theta_{B-D^*\ell}$ fit, while the LEP collaborations use a model constrained by LEP measurements of $\bar{B} \to D^*X\ell\nu$.

In order to derive $|V_{cb}|$ from the measured value of $|V_{cb}|\mathcal{F}_{D^*}(1)$, we use

$$\mathcal{F}_{D^*}(1) = 0.913 \pm 0.042 \qquad (26)$$

from the BABAR Physics Book [31] and obtain

$$|V_{cb}| = (46.2 \pm 1.4 \pm 2.0 \pm 2.1) \times 10^{-3} \qquad (27)$$

where the errors are statistical, systematic, and due to the uncertainty in $\mathcal{F}_{D^*}(1)$. The difference between this result and the inclusive measurement (Eq. (14)) may indicate a breakdown of quark-hadron duality in inclusive semileptonic B decays.

7 Preliminary CLEO III Results on Rare B Decays

Previously CLEO measured the branching fractions for the four possible $B \to K\pi$ modes and $B \to \pi^+\pi^-$, and determined comparable upper limits for the other $B \to \pi\pi$ modes and for $B \to K\bar{K}$ decays [32,33,34]. These exclusive two-body B decays are very important because:

- Certain ratios of $B \to K\pi$ branching fractions depend [35,36] explicitly on the angle $\gamma = \arg(V_{ub}^*)$ of the unitarity triangle (Figure 1). The modest dependence of these ratios on models suggests that γ can be obtained from fits to comprehensive measurements of these branching fractions.
- The sum of the angles β and γ (Figure 1) can also be determined from time-dependent CP violation measurements in $B^0 \to \pi^+\pi^-$ decays. This requires separation of penguin contributions from tree contributions to the decay using isospin analysis [37] of all three $B \to \pi\pi$ charge states.

- Whether or not the CP violating phase in the CKM matrix is the sole source of CP violation is still an open question. Self tagging rare decay modes such as $B^+ \to K^+\pi^0$ are an obvious arena in which to search for other manifestations of CP violation.

Hence, these rare B decays can play particularly important roles in constraining the CKM matrix and developing our understanding of CP violation.

Only CLEO II and CLEO II.V data were used in previous CLEO measurements of these B decays. CLEO now has *preliminary* measurements of branching fractions or determinations of upper limits for $B \to K\pi$, $B \to \pi\pi$, $B \to K\bar{K}$, and $B^- \to D^0K^-$ decays, from about one-half of the CLEO III data. This is the first public presentation of these results.

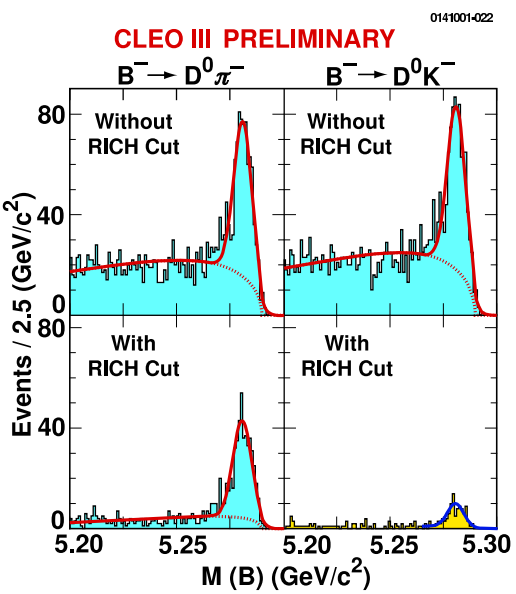

Figure 15. Preliminary CLEO III mass distributions for $B^- \to D^0\pi^-$ and $B^- \to D^0K^-$ candidates, without and with use of information from the RICH detector for K/π separation.

The key to these new measurements is the excellent performance of the CLEO III tracking system and RICH detector. The RICH provides very clean K/π separation at the momenta ($p \sim 2.5$ GeV/c) of the kaons and pions from $B \to K\pi$, $\pi\pi$ and $K\bar{K}$ decay, *e.g.*, within the fiducial volume (80% of 4π), the K efficiency is 85% with a 5% π fake rate.

The power of the RICH in reconstructing rare B decays is illustrated in Figure 15 which shows the B mass peaks for $B^- \to D^0\pi^-$ and $B^- \to D^0K^-$ candidates with and without using information from the RICH. Without the RICH, the signal for the Cabibbo suppressed $B^- \to D^0K^-$ mode is overwhelmed with background from the Cabibbo favored $B^- \to D^0\pi^-$ decay. With the RICH, the $B^- \to D^0K^-$ signal is almost free of background. The previous CLEO measurement of $\mathcal{B}(B^- \to D^0K^-)$ required a very sophisticated analysis, while the CLEO III measurement is simple and straight-forward. The *preliminary* CLEO III branching fraction

$$\mathcal{B}(B^- \to D^0K^-) = (3.8 \pm 1.3) \times 10^{-4} \quad (28)$$

agrees very well with the earlier CLEO result [38]

$$\mathcal{B}(B^- \to D^0K^-) = (2.6 \pm 0.7) \times 10^{-4}. \quad (29)$$

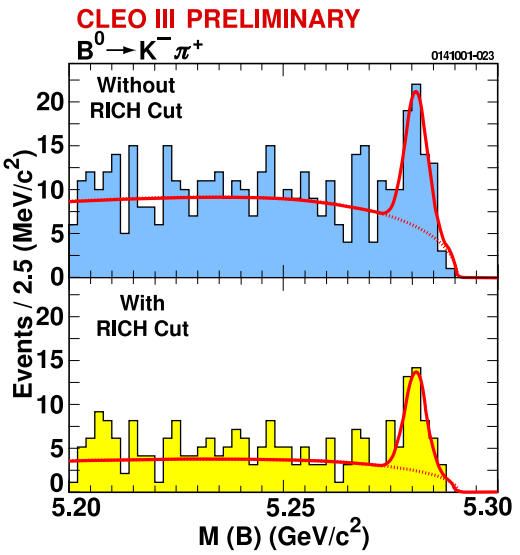

Figure 16. Reconstruction of $B^0 \to K^-\pi^+$ decays using the RICH detector. The top and bottom figures illustrates the $K\pi$ mass peaks without and with using information from the RICH.

Figure 16 shows that the RICH detector is also very effective in reducing backgrounds

Table 3. CLEO measurements of charmless two-body B meson decays. For each decay mode, the first row is the *preliminary* CLEO III result and the second row is the previously published result from CLEO II and CLEO II.V data [33,34]. Upper limits (UL) are at the 90% CL.

Mode	Efficiency	Yield	Significance	$\mathcal{B}$ (10^{-6})	UL (10^{-6})
$K^{\pm}\pi^{\mp}$	46%	$29.2^{+7.1}_{-6.4}$	5.4σ	$18.6^{+4.5+3.0}_{-4.1-3.4}$	
	48%	$80.2^{+11.8}_{-11.0}$	11.7σ	$17.2^{+2.5}_{-2.4} \pm 1.2$	
$K^{\pm}\pi^{0}$	32%	$12.9^{+6.5}_{-5.5}$	3.8σ	$13.1^{+5.8+2.8}_{-4.9-2.9}$	
	38%	$42.1^{+10.9}_{-9.9}$	6.1σ	$11.6^{+3.0+1.4}_{-2.7-1.3}$	
$K^{0}\pi^{\pm}$	12%	$14.8^{+4.9}_{-4.1}$	6.2σ	$35.7^{+12\ +5.4}_{-9.9-6.2}$	
	14%	$25.2^{+6.4}_{-5.6}$	7.6σ	$18.2^{+4.6}_{-4.0} \pm 1.6$	
$K^{0}\pi^{0}$	8.5%	$3.0^{+2.9}_{-2.5}$	1.6σ	$10.4^{+10\ +2.9}_{-8.3-2.9}$	
	11%	$16.1^{+5.9}_{-5.0}$	4.9σ	$14.6^{+5.9+2.4}_{-5.1-3.3}$	
$\pi^{\pm}\pi^{\mp}$	35%	$3.9^{+1.5}_{-1.2}$	2.2σ	$3.2^{+3.3+1.0}_{-2.5-1.0}$	
	48%	$20.0^{+7.6}_{-6.5}$	4.2σ	$4.3^{+1.6}_{-1.4} \pm 0.5$	
$\pi^{\pm}\pi^{0}$	29%	$11.5^{+5.6}_{-4.5}$	3.4σ	$11.7^{+5.7+2.2}_{-4.6-2.4}$	
	39%	$21.3^{+9.7}_{-8.5}$	3.2σ		12.7
$\pi^{0}\pi^{0}$	29%	$2.7^{+2.4}_{-1.6}$	2.9σ		11
	29%	$6.2^{+4.8}_{-3.7}$	2.0σ		5.7
$K^{\pm}K^{\mp}$	36%	$1.0^{+2.4}_{-1.7}$	0.6σ		4.5
	48%	$0.7^{+3.4}_{-0.7}$	0.0σ		1.9
$K^{0}K^{\pm}$	12%	$0.5^{+1.9}_{-1.1}$	0.8σ		18
	14%	$1.4^{+2.4}_{-1.3}$	1.1σ		5.1
$K^{0}\bar{K^{0}}$	13%	$0.0^{+0.5}_{-0.5}$	0.0σ		13
	5%	0	0.0σ		17

and improving the signal to noise ratio in $B^0 \to K^+\pi^-$ decays.

The other techniques used in reconstructing these decays are similar to those used in the previous CLEO analyses [32,33,34]. The *preliminary* results from CLEO III data are compared to the previous CLEO measurements in Table 3. In all cases the CLEO III results agree very well with the earlier CLEO measurements. The final results from the full CLEO III data sample will be combined with the earlier CLEO measurements.

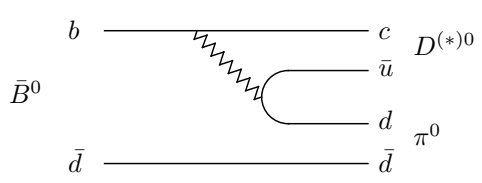

Figure 17. The internal spectator diagram for $\bar{B} \to D^{(*)0}\pi^0$ decay.

8 Other Recent CLEO Results

In this section I briefly mention a few other recent CLEO results.

Internal spectator diagrams (see Figure 17) in $\bar{B}$ decay are processes in which the W from $b \to c(u)$ decay produces a $q\bar{q}'$ pair that hadronizes with $c(u)$ quark and the antiquark from the $\bar{B}$. These decays are suppressed because the color of the $q\bar{q}'$ quarks does not automatically match the colors in the quarks from the $\bar{B}$ fragment. So far the only color suppressed $\bar{B}$ decays that have

been observed have charmonium in the final state, *e.g.*, $\bar{B}^0 \to J/\psi \bar{K}^0$. CLEO has now observed [39] the first color suppressed decays without charmonium in the final state, $\bar{B}^0 \to D^0\pi^0$ and $\bar{B}^0 \to D^{*0}\pi^0$.

The branching fractions measured for these decays are

$$\mathcal{B}(\bar{B}^0 \to D^0\ \pi^0) = (2.74^{+0.36}_{-0.32} \pm 0.55) \times 10^{-4} \quad \text{and} \tag{30}$$

$$\mathcal{B}(\bar{B}^0 \to D^{*0}\pi^0) = (2.20^{+0.59}_{-0.52} \pm 0.79) \times 10^{-4}. \tag{31}$$

The statistical significances of these signals are 12σ and 5.9σ for $D^0\pi^0$ and $D^{*0}\pi^0$, respectively.

CLEO studies of $B \to K\pi$ and $B \to \pi\pi$ decays demonstrated that gluonic penguin diagrams are important in B decay (see Section 7). However, final states such as $B \to \phi K$ and $B \to \phi K^*$ play a special role since they cannot be produced at a significant rate by any other decay mechanism. Earlier, CLEO reported [40] the first significant measurement of some of these decays. The branching fractions,

$$\mathcal{B}(B^- \to \phi K^-) = (5.5^{+2.1}_{-1.8} \pm 0.6) \times 10^{-6} \tag{32}$$

and

$$\mathcal{B}(B^0 \to \phi K^{*0}) = (11.5^{+4.5+1.8}_{-3.7-1.7}) \times 10^{-6}, \tag{33}$$

were measured at significance levels of 5.4σ and 5.1σ, respectively. These branching fractions are well within the rather large ranges predicted by theoretical models (see Ref. [40]). Indications of the other charge modes, ϕK^0 and ϕK^{*-}, were observed at the $\sim 3\sigma$ level.

The FCNC decays $B \to K\ell^+\ell^-$ and $B \to K^*\ell^+\ell^-$ are another window on effects from possible New Physics in radiative penguin loops, since the γ in $\ell^+\ell^-$ decays is virtual. In particular, $B \to K\gamma$ is forbidden by angular momentum conservation, while $B \to K\ell^+\ell^-$ is allowed. So far these exclusive decays have not been observed. CLEO recently reported [41] improved upper limits

$$\mathcal{B}(B \to K\ \ell^+\ell^-) < 1.7 \times 10^{-6} \quad \text{and} \tag{34}$$

$$\mathcal{B}(B \to K^*\ell^+\ell^-) < 3.3 \times 10^{-6} \tag{35}$$

at the 90% CL. (For the $\mathcal{B}(B \to K^*\ell^+\ell^-)$ limit, the dilepton mass range is $m_{\ell\ell} > 0.5$ GeV.) The limit, $\mathcal{B}(B \to K^{(*)}\ \ell^+\ell^-) < 1.5 \times 10^{-6}$, obtained for the weighted average of these decays, is not very far above the theoretical prediction [42]: 1.0×10^{-6}.

The decay $B^+ \to D^{*+}K^0_S$ should proceed via an annihilation diagram in which the W^+ from the annihilation of the $\bar{b}$ and u quarks produces a $c\bar{s}$ pair which hadronizes to $D^{*+}K^0_S$. No reliable theoretical prediction for the rate of this decay exists. We searched [43] for this decay and determined an upper limit at the 90% CL:

$$\mathcal{B}(B^+ \to D^{*+}K^0_S) < 9.5 \times 10^{-5} \tag{36}$$

9 CLEO-c and CESR-c

CLEO-c is a focused program of measurements and searches in e^+e^- collisions in the the $\sqrt{s} = 3 - 5$ GeV energy region [44]. Topics to be studied include:

- Precision – $\mathcal{O}(1\%)$ – charm measurements: absolute charm branching fractions, the decay constants f_{D^+} and f_{D_s}, semileptonic decay form factors, and the CKM matrix elements $|V_{cd}|$ and $|V_{cs}|$
- Searches for New Physics in the charm sector: CP violation in D decay, $D\bar{D}$ mixing without doubly suppressed Cabibbo decay, and rare D decays
- τ studies: precision measurements and searches for New Physics
- QCD studies: $c\bar{c}$ spectroscopy, searches for glue-rich exotic states (glueballs and hybrids), and measurements of R (direct between 3 and 5 GeV, and indirect using initial state radiation between 1 and 3 GeV)

The CLEO III detector described above is a crucial element of this program. Its capabilities and performance are substantially beyond those of other detectors that have operated in the charm threshold region.

Testing Lattice QCD (LQCD) calculations with precision measurements is a major

emphasis of the CLEO-c program. Theoretical analysis of strongly-coupled, nonperturbative quantum field theories remains one of the foremost challenges in modern physics. Experimental progress in flavor physics (*e.g.*, determining the CKM matrix elements $|V_{cb}|$, $|V_{ub}|$, and $|V_{td}|$) is frequently limited by knowledge of nonperturbative QCD effects, (*e.g.*, decay constants and semileptonic form factors). (One sort of approach to reducing theoretical uncertainties in determining $|V_{cb}|$ and $|V_{ub}|$ was already described in Secs. 4 and 5.) In the last decade several technical problems in LQCD have been identified and overcome, and substantially improved algorithms have been developed. LQCD theorists are now poised to move from $\mathcal{O}(15\%)$ precision to $\mathcal{O}(1\%)$ precision in calculating many important parameters that can be measured experimentally or are needed to interpret experimental measurements, including:

- masses, leptonic widths, EM transition form factors, and mixing amplitudes of $c\bar{c}$ and $b\bar{b}$ bound states; and
- masses, decay constants, and semileptonic decay form factors of D and B mesons.

CLEO-c will provide data in the charm sector to motivate and validate many of these calculations. This will help to establish a comprehensive mastery of nonperturbative QCD, and enhance confidence in LQCD calculations in the beauty sector.

The CLEO-c program is based on a four-year run plan, where the first year is spent on the Υ resonances while constructing hardware for CESR improvements. We expect to accumulate the following data samples:

2002 $\gtrsim$1 fb^{-1} at each of the $\Upsilon(1S)$, $\Upsilon(2S)$, $\Upsilon(3S)$ resonances
(10-20 times the existing world's data)

2003 3 fb^{-1} at the $\psi(3770)$ – 30 M $D\bar{D}$ events and 6 M tagged D decays
(310 times the MARK III data)

2004 3 fb^{-1} at $\sqrt{s} \sim 4.1$ GeV – 1.5 M $D_s\bar{D}_s$ events and 0.3 M tagged D_s decays
(480 times the MARK III data and 130 times the BES II data)

2005 1 fb^{-1} at the J/ψ – 1 G J/ψ decays
(170 times the MARK III data and 20 times the BES II data)

Detailed Monte Carlo simulations show that we will be able to measure the charm reference branching fractions, decay constants, slopes of semileptonic form factors, and CKM matrix elements – all with $\mathcal{O}(1\%)$ precision.

Goals of the run on the Υ bound states include searches for the "missing $b\bar{b}$ states" – *e.g.*, $^1S_0$ ($\eta_b, \ldots$) and $^1P_1$ ($h_b, \ldots$) – and accurate measurements of Γ_{ee}'s, transition rates, and hyperfine splittings. Most of the quantities that will be measured in this program can be used to validate precise LQCD calculations.

The 1 G J/ψ events will be an extremely rich source of data for glueball searches. The very controversial $f_J(2220)$ is an excellent example of the enormous reach of this program. Using the values of $\mathcal{B}(J/\psi \to \gamma f_J)\mathcal{B}(f_J \to Y\bar{Y})$ measured by BES [45] we expect peaks with 23,000, 13,000, and 15,600 events would be observed in the $f_J(2220)$ decay channels $\pi^+\pi^-$, $\pi^0\pi^0$, and K^+K^-, respectively. All of these signals would stand out well above reasonable estimates of backgrounds.

We have just completed the installation of superconducting interaction region quadrupoles that will allow us to operate CESR over the energy range from charm threshold to above the $\Upsilon(4S)$. In the Υ region, synchrotron radiation damping reduces the size of beams in CESR and is a crucial factor for achieving high luminosity. This damping will be much less at lower energies in the charm threshold region, and that would substantially reduce luminosity. Much of this luminosity loss can be recovered by installing wiggler magnets (magnets with alternating magnetic field directions) to increase synchrotron radiation. We plan to use superferric wiggler magnets (Fe poles and superconducting coils) and we have already con-

structed a three-pole prototype. The anticipated luminosity will still be below that achieved in the Υ region, and will increase with energy, ranging from 0.2×10^{33} cm^{-2} s^{-1} to 0.4×10^{33} cm^{-2} s^{-1} in the energy region between 3.1 and 4.1 GeV, and rising to $\gtrsim 1 \times 10^{33}$ cm^{-2} s^{-1} in the Υ region. These wiggler magnets are the only substantial CESR hardware upgrade required for the CLEO-c program, and – not entirely incidentally – they are also excellent prototypes for the wiggler magnets that would be needed in linear collider damping rings.

10 Summary and Conclusions

We report new results based on the full CLEO II and CLEO II.V data samples. For $b \to s\,\gamma$ decays we find

$$\mathcal{B}(b \to s\,\gamma) = (3.21 \pm 0.43 \pm 0.27^{+0.18}_{-0.10}) \times 10^{-4} \quad (37)$$

where the first error is statistical, the second is systematic, and the third is from theoretical corrections. We substantially reduced the theoretical uncertainties that occurred in our earlier measurement [9] by including nearly all of the photon energy spectrum. We measured $|V_{cb}|$ using $\bar{B} \to X_c \ell \bar{\nu}$ hadronic mass moments and $b \to s\,\gamma$ energy moments, again with substantially reduced theoretical uncertainties. The result is

$$|V_{cb}| = (40.4 \pm 0.9 \pm 0.5 \pm 0.8) \times 10^{-3} \quad (38)$$

where the errors are due to uncertainties in moments, Γ^c_{SL}, and theory, in that order. We measured $|V_{ub}|$ using the $b \to s\,\gamma$ spectrum to determine the fraction of the $\bar{B} \to X_u \ell \bar{\nu}$ lepton momentum spectrum in the momentum interval used. The *preliminary* result is

$$V_{ub} = (4.09 \pm 0.14 \pm 0.66) \times 10^{-3} \quad (39)$$

where the first error is statistical and the second is systematic. Again, theoretical uncertainties are substantially less than those in previous measurements.

We report a *preliminary* new measurement of $|V_{cb}|$ from both $\bar{B}^0 \to D^{*+} \ell^- \bar{\nu}$ and $B^- \to D^{*0} \ell^- \bar{\nu}$ decays. The result is

$$|V_{cb}| = (46.2 \pm 1.4 \pm 2.0 \pm 2.1) \times 10^{-3} \quad (40)$$

where the errors are statistical, systematic, and theoretical, respectively.

We present the first *preliminary* results from CLEO III data – measurements of and upper limits for $\mathcal{B}(B \to K\pi)$, $\mathcal{B}(B \to \pi\pi)$, and $\mathcal{B}(B \to K\bar{K})$.

Finally, we are embarking on a new program of operating CESR and CLEO at the Υ bound states and in the charm threshold region. This program will yield: precision measurements of Υ parameters, searches for missing $b\bar{b}$ states, precision measurements in the charm and tau sectors, searches for New Physics in charm and tau decays, and definitive searches for low-lying glueball states. This diverse program will be unified by collaboration with Lattice QCD theorists who will use the results to validate their calculations and gain confidence for their utilization in the b quark sector.

Acknowledgments

I am delighted to express my appreciation for my CESR and CLEO colleagues whose effort provided the results described here, and for the contributions of our theoretical colleagues to these measurements. Our research was supported by the NSF and DOE. I appreciate the hospitality of the DESY Hamburg laboratory where I prepared this report for the conference proceedings. Fabio Anulli provided invaluable assistance in his role as Scientific Secretary. Finally, I want to thank Paolo Franzini, Juliet Lee-Franzini, and the entire staff of Lepton-Photon 2001 for the delightful conference that they organized.

References

1. H. Tajima, these proceedings.
2. J. Nash, these proceedings.
3. M. Neubert, these proceedings.
4. R. Barbieri, these proceedings.
5. M. Wise, these proceedings.

6. G. Isidori, these proceedings.
7. J. Dorfan, these proceedings.
8. S. Olsen, these proceedings.
9. CLEO Collaboration, M.S. Alam *et al.*, *Phys. Rev. Lett.* **74**, 2885 (1995).
10. CLEO Collaboration, S. Chen *et al.*, Cornell Report No. 01/1751, CLEO 01-16 (2001), hep-ex/0108032, *Phys. Rev. Lett. (to be published).*
11. *A. Ali and C. Greub, Phys. Lett. B* **259**, *182 (1991).*
12. *A.L. Kagan and M. Neubert, E. Phys J. C* **7**, *5 (1999).*
13. *ALEPH Collaboration, R. Barante et al., Phys. Lett. B* **429**, *169 (1998).*
14. *Belle Collaboration, K. Abe et al., Phys. Lett. B* **511**, *151 (2001).*
15. *K. Chetyrkin, M. Misiak, and M. Münz, Phys. Lett. B* **400**, *206 (1997).*
16. *P. Gambino and M. Misiak, hep-ph/01404034.*
17. *D. Cronin-Hennessy et al., Cornell Report No. CLNS 01/1752, CLEO 01-17 (2001), hep-ex/0108033, Phys. Rev. Lett. (to be published).*
18. *A. Falk and M. Luke, Phys. Rev. D* **57**, *424 (1998) and private communication.*
19. *CLEO Collaboration, B. Barish et al., Phys. Rev. Lett.* **76**, *1570 (1996).*
20. *CLEO Collaboration, J.P. Alexander et al., Phys. Rev. Lett.* **86**, *2737 (2001).*
21. *Particle Data Group, D.E. Groom et al., E. Phys J. C* **15**, *1 (2000).*
22. *F. De Fazio and M. Neubert, JHEP* **06**, *017 (1999).*
23. *A.H. Hoang, Z. Ligeti, and A.V. Manohar, Phys. Rev. D* **59**, *074017 (1999).*
24. *N. Uraltsev, Int. J. Mod. Phys. A* **14**, *4641 (1999).*
25. *CLEO Collaboration, J. Bartelt et al., Phys. Rev. Lett.* **71**, *4111 (1993).*
26. *M. Neubert, Phys. Rep.* **245**, *259 (1994).*
27. *I. Caprini, L. Lellouch, and M. Neubert, Nucl. Phys. B* **530**, *153 (1998).*
28. *CLEO Collaboration, J. Duboscq et al., Phys. Rev. Lett.* **76**, *3898 (1996).*
29. *K.M. Ecklund and D. Cinabro in the Proceedings of the XXXth International Conference on High Energy Physics, July 27 - August 2, 2000, Osaka, Japan.*
30. *LEP data are summarized and corrected to common daughter branching fractions by the LEP Heavy Flavor Working Group*
31. *The* BaBar *Physics Book, editors P.F. Harison and H.R. Quinn, SLAC Report No. SLAC-R-504 (1998).*
32. *CLEO Collaboration, R. Godang et al., Phys. Rev. Lett.* **80**, *3456 (1998).*
33. *CLEO Collaboration, D. Cronin-Hennessy et al., Phys. Rev. Lett.* **85**, *515 (2000).*
34. *CLEO Collaboration, D.M. Asner et al., Cornell Report No. CLNS 01/1718, CLEO 01-02 (2001).*
35. *See Ref.* [33] *for references to the original literature.*
36. *M. Beneke, G. Buchalla, M. Neubert, and C.T. Sachrajda, Nucl. Phys. B* **606**, *245 (2001).*
37. *M. Gronau and D. London, Phys. Rev. Lett.* **65**, *3381 (1990).*
38. *CLEO Collaboration, M. Athanas et al., Phys. Rev. Lett.* **80**, *5493 (.)*
39. *CLEO Collaboration, T.E. Coan et al., Cornell Report No. CLNS 01/1755, CLEO 01-18 (2001).*
40. *CLEO Collaboration, R.A. Briere et al., Phys. Rev. Lett.* **86**, *3718 (2001).*
41. *CLEO Collaboration, S. Anderson et al., Phys. Rev. Lett.* **87**, *181803 (2001).*
42. *A. Ali, P. Ball, L.T. Handoko, and G. Hiller, Phys. Rev. D* **61**, *074024 (2000).*
43. *CLEO Collaboration, A. Gritsan et al., Phys. Rev. D* **64**, *077501 (2001)*
44. *CLEO-c Taskforce, CESR-c Taskforce, and CLEO-c Collaboration, Cornell Report No. CLNS 01/1742 (2001), Revised 10/2001. Links to electronic copies are available at:*
`http://www.lns.cornell.edu/` .
45. *BES Collaboration, Z.J. Bai et al., Phys. Rev. Lett.* **76**, *3502 (1996).*